Ballistic conductance and thermoelectric power of lead-salt semiconductor nanowires

V. Aparecida da Costa and E. A. de Andrada e Silva*
Instituto Nacional de Pesquisas Espaciais (INPE), CP 515, 12201-970 São José dos Campos, SP, Brazil
(Received 26 May 2010; published 11 October 2010)

With a three-dimensional model for lead-salt nanowires (NWs) and an accurate description of the bulk band structure near the gap, we study the electronic contribution to the thermoelectric properties of these NWs in the ballistic transport regime. The electronic conductance and thermopower (or Seebeck coefficient) are calculated as a function of the wire's dimensions, temperature, and carrier concentration using the linear response Landauer quantum-transport theory. The single-particle energy states are determined within the envelope function approximation using Dimmock's four-band $k\cdot p$ model for the bulk. Specific numerical results are shown for [110] PbTe NWs. The thermoelectric response of lead-salt NWs is shown to be characterized by irregular oscillations, even in the case of ideal wire and contacts, due to the intrinsic band anisotropy and break of valley degeneracy, independent of the NW crystallographic orientation.

DOI: 10.1103/PhysRevB.82.153302 PACS number(s): 73.63.−b, 72.20.Pa, 73.21.Hb, 73.23.Ad

Semiconductor nanostructures have been shown to present great possibilities for new thermoelectric devices.[1–3] In particular, PbTe nanostructures have been intensively investigated due to the good thermoelectric response of the lead salts (PbTe, PbSe, and PbS) and to the recent advances in their fabrication with molecular beam epitaxy[4,5] and electron-beam lithography.[6,7] Enhancement of the thermoelectric figure of merit has been reported for PbTe/PbSeTe superlattice (SL);[8] the thermoelectric power of PbTe/PbEuTe multiple quantum wells has been investigated in detail in Ref. 9, and the thermoelectric properties of PbTe SL nanowires (NWs) (Refs. 9 and 10) and PbTe nanocomposites[11] have also been studied. In these studies, the thermoelectric transport has been considered in the semiclassical regime, and the nonparabolicity and multiple valley (or pocket) structure of the PbTe conduction and valence bands have often been neglected.

Despite the fact that PbTe is a good material for both thermoelectric[12] and quantum ballistic devices,[6,7] the ballistic thermoelectric transport coefficients of PbTe nanowires seem to have not been studied yet. Such thermoelectric ballistic transport has been used in mesoscopic studies[13–16] with two-dimensional (2D) models for the wire or quantum constriction, which lead to a wire's thermoelectric power characterized by regular oscillations. More recently, it has been also used in the macroscopic limit and to compare performances in different dimensions.[17] In this Brief Report, we discuss the ballistic conductance and thermoelectric power (or Seebeck coefficient) of realistic three-dimensional (3D) lead-salt nanowires including band nonparabolicity, anisotropy, and multivalley effects. The multiband envelope function approximation based on Dimmock's four-band $k\cdot p$ model[18] is employed in the NW electronic-structure calculation.

Let us consider lead-salt NWs with square cross section of side L connected on both ends by metallic contacts at temperature T and with Fermi energy E_F. A small electric bias (V) and temperature difference (ΔT) is then assumed between these contacts, (i.e., $eV \ll E_F$ and $\Delta T \ll T$) and the electronic conductance (G) and thermoelectric power (S) are computed within the linear response regime using the two-probe Landauer formula.[19] We further simplify and assume ideal (i.e., reflectionless) contacts so that the electron transmission is one for every open conducting channel (or subband) in the NW.[20] The thermoelectric transport coefficients in this case will be as in a point contact, dependent only on the wire cross section, i.e., on the 2D confining potential. The conductance and thermoelectric power in this case are given, respectively, by[14,15,17]

$$G(L,E_F,T) = (2e^2/h)L_0 \tag{1}$$

and

$$S(L,E_F,T) = -(k_B/e)L_1/L_0, \tag{2}$$

where

$$L_{\nu=0,1} = -\sum_{nm\mu}\int_0^\infty dE\frac{df}{dE}\left(\frac{E-E_F}{k_BT}\right)^\nu \Theta[E-\varepsilon_{nm}^{(\mu)}(L)] \tag{3}$$

being $f=[\exp(\frac{E-E_F}{k_BT})+1]^{-1}$ the Fermi-Dirac distribution and Θ the usual Heaviside step function. $\varepsilon_{nm}^{(\mu)}(L)$ gives the energies of the conducting channels in the semiconductor NW, (nm) being the quantum numbers of the two-dimensional confinement and μ the valley index. Independent valleys are assumed. After integration, one gets

$$G = \frac{2e^2}{h}\sum_{nm\mu} f(\epsilon_{nm}^{(\mu)}) \tag{4}$$

and

$$S = -\frac{k_B}{e}\frac{\sum_{nm\mu}[\ln(1+e^{-\epsilon_{nm}^{(\mu)}}) + \epsilon_{nm}^{(\mu)}(1+e^{\epsilon_{nm}^{(\mu)}})^{-1}]}{\sum_{nm\mu} f(\epsilon_{nm}^{(\mu)})} \tag{5}$$

with $\epsilon_{nm}^{(\mu)}=\frac{\varepsilon_{nm}^{(\mu)}-E_F}{k_BT}$. The above expressions show the explicit dependence of G and S on the valley-dependent NW electronic structure $\varepsilon_{nm}^{(\mu)}$, which is now calculated, and differ from those obtained in Ref. 15 only by the summation over the different valleys and over the extra quantum number due to the present 3D model for the NW.

To obtain the NW electronic structure we start from Dimmock's $k\cdot p$ model for the bulk, which leads to an effective

Schrodinger equation ($H_E=EF$) for the envelope function $F(y,z)$ (with total function $\Psi=Fe^{ik_x x}$) of quantized states for electrons and/or holes confined in the NW, i.e., free to move only along the wire axis ($\|x$) with the following energy-dependent effective Hamiltonian:

$$H_E = -\frac{\hbar^2}{2}\frac{d}{dy}\frac{1}{m_y^{(\mu)}}\frac{E_g}{E+E_g}\frac{d}{dy} - \frac{\hbar^2}{2}\frac{d}{dz}\frac{1}{m_z^{(\mu)}}\frac{E_g}{E+E_g}\frac{d}{dz} + V, \quad (6)$$

where y and z are parallel to the main axis of the 2D effective mass tensor with corresponding band edge effective masses $m_y^{(\mu)}$ and $m_z^{(\mu)}$ (for electrons or holes in the μ valley); the energy is measured from the band edge, and E_g and $V=V(y,z)$ stand for the band-gap energy and for the confining potential, as given by the band offsets and/or applied electrostatic potentials [note that, in general, $E_g=E_g(y,z)$ and $m_i^{(\mu)}=m_i^{(\mu)}(y,z)$, $i=y,z$]. H_E in Eq. (6) is obtained from the projection of the four-band Dimmock $k\cdot p$ model into the conduction (or valence) band.[21] Such model describes well the band-gap region of all lead salts and has been shown to be quantitatively valid in the interpretation of optical absorption data of PbTe quantum wells[4,5] and quantum dots.[22] It presents solutions for discrete values of $E=\varepsilon_{nm}^{(\mu)}$, corresponding to the energies of the above-mentioned transport channels. In most of the cases, Eq. (6) must be solved numerically. However, due to the paraelectric properties of lead salts, corresponding to huge dielectric constants, the band bending can be usually neglected in PbTe nanostructures, and a simple analytical but yet accurate solution is possible for the present square PbTe NWs in the case of strong confinement (i.e., large band offsets), which can be easily obtained with vacuum or PbEuTe barriers. In this case, for the lower lying energy states one can assume infinite barriers, eventually with an effective confinement width $L_{eff.}$, slightly large then L, to simulate the barrier penetration. The effective Hamiltonian above becomes then separable with eigenfunctions given by $F_{nm}=A\sin(\frac{n\pi}{L}y)\sin(\frac{m\pi}{L}z)$, independent of the valley. The corresponding energy eigenvalues which are valley dependent are then given by

$$\varepsilon_{nm}^{(\mu)} = -\frac{E_g}{2}\left(1-\sqrt{1+\frac{2\hbar^2}{m_x^{(\mu)}}\frac{k_{nm}^{(\mu)2}}{E_g}}\right), \quad (7)$$

where

$$k_{nm}^{(\mu)2} = \frac{m_x^{(\mu)}}{m_y^{(\mu)}}\left(\frac{n\pi}{L}\right)^2 + \frac{m_x^{(\mu)}}{m_z^{(\mu)}}\left(\frac{m\pi}{L}\right)^2. \quad (8)$$

Note that even though $\varepsilon_{nm}^{(\mu)}$ does not depend on $m_x^{(\mu)}$, the introduction of $k_{nm}^{(\mu)}$ helps further and practical calculations—see, for example, Eq. (9) below. Therefore, all one needs to do now is to insert the effective masses for each type valley into the above result for $\epsilon_{nm}^{(\mu)}$, and then perform the summations in Eqs. (4) and (5) to obtain straightforwardly both G and S.

As a specific example, we now consider the ballistic thermoelectric transport along [110] PbTe NWs, as a function of the wire's width L, carrier concentration and temperature. These NWs can be fabricated from [001] PbTe quantum wells, grown for example on top of NaCl substrates and

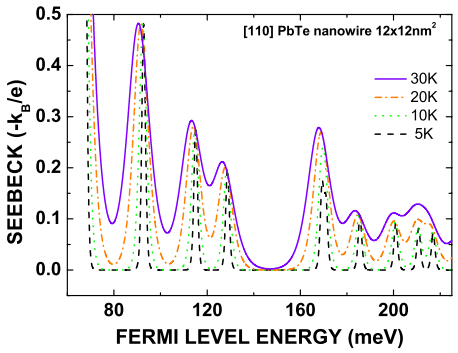

FIG. 1. (Color online) Obtained thermoelectric power, or Seebeck coefficient, for a 12×12 nm^2 [110] PbTe nanowire, at different temperatures, as a function of the Fermi energy in metallic contacts.

serve as a simple example for the effects of anisotropy and break of valley degeneracy, which occurs in every lead-salt NW regardless of its crystallographic orientation. We first recall that the four equivalent valleys of the lead-salt bulk band-gap structure, along the [111] directions, remain equivalent (or degenerate) in [001] QWs.[21] Due to further confinement in a [110] NW, these four valleys split into two pairs: one of valleys with the main axis along the wire (i.e., $\|$[110]), called longitudinal valleys ($\mu=l$), and one of valleys with the main axis perpendicular to the wire, called transverse valleys ($\mu=t$). In units of the free electron mass, the corresponding low-temperature conduction-band edge effective masses for PbTe used in the present calculations were:[21,23] $m_x^{(t)}=0.024$, $m_y^{(t)}=0.168$, $m_z^{(t)}=0.034$ and $m_x^{(l)}=0.168$, $m_y^{(l)}=0.024$, $m_z^{(l)}=0.034$. Note that, due to the structure's symmetry, the effective mass along the growth direction is the same in both types of valleys, while $m_x^{(\mu)}$ and $m_y^{(\mu)}$ are exchanged, and that, in this two-band model, the band-edge effective mass is proportional to the band gap, and the above values correspond to low-temperature $E_g\sim190$ meV. $E_g(T)$ indicates the value of the energy gap at each temperature considered. In the present linear transport regime, since $\Delta T\ll T$ and E_g is a smooth function of T, it can be safely assumed constant, as a true parameter of the model. In these calculations we have used $E_g(T)=189.7+0.45T^2/(T+50)$ meV.[4,5]

The thermoelectric power spectrum of a [110] square PbTe NW with $L=12$ nm at different temperatures is shown in Fig. 1. As expected, in this range of temperature, the thermoelectric power presents sharp peaks connected to the discrete set of conducting channels allowed in the wire. Large independent peaks are seen up to $T=30$ K, temperature in which the conductance steps are already almost washed out. Note also that the temperature dependence comes from both the variations in the occupancy of the states and in band parameters. It is somewhat surprising though that, despite considering ideal wires with ideal contacts, very irregular oscillations in the thermoelectric power of these PbTe NWs are predicted. It differs from the results of previous mesoscopic studies with 2D models, where the thermoelectric power always presents regular oscillations, with monotonically decreasing peak intensity.[13–16] As shown below, these

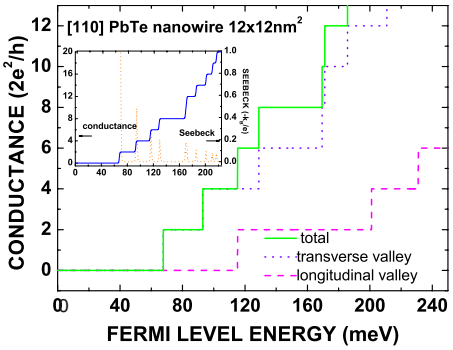

FIG. 2. (Color online) Low-temperature electron conductance of a 12×12 nm^2 [110] PbTe nanowire. The separate contributions from the transverse (doted line) and longitudinal valleys (dashed line) are also shown. The inset plots G and S together and explicit shows their relation.

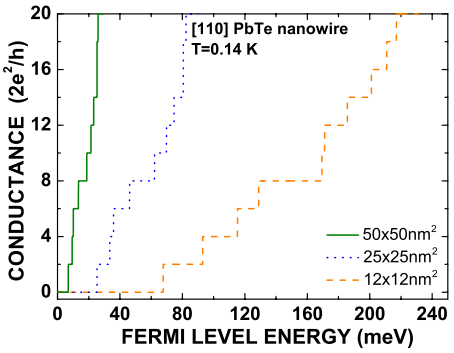

FIG. 3. (Color online) Conductance of [110] PbTe nanowires of three different sizes (i.e., L): 12×12 nm^2 (dashed line), 25×25 nm^2 (doted line), and 50×50 nm^2 (continue line).

irregularities are due to the band anisotropy and multivalley structure of the lead salts, and are expected to show up in lead-salt NWs along any direction, due to the break of valley degeneracy.

Figure 2 shows the low-temperature conductance obtained for the same wire of Fig. 1, as well as the separate contributions from the two nonequivalent pairs of valleys. Such low-temperature wire conductance in [110] PbTe NWs increases with steps of $4e^2/h$ due to spin *and* valley degeneracy. The inset plots together G and S and shows the thermoelectric peaks at the onset of each new conducting channel. The conductance step length is seen to vary with E_F and with the type of valley. Due to the different effective masses, the two types of valleys lead to two different and incommensurate series of energy levels. When these two series of levels are added together, as in the calculation of G and S, the irregular oscillations in Fig. 1 are obtained. Therefore by choosing the wire width L (or, for a rectangular wire, L_z and L_y independently), the allowed states for electrons in the NW can be made to form quasidegenerate groups of states near E_F, in order to enhance the thermopower at the corresponding carrier concentration.

For a given E_F, the carrier density in the wire is calculated by summing the carrier concentration over all occupied subbands and valleys. From Eq. (7), one can easily calculate the density of states and the carrier concentration in each conducting channel. For example, the carrier concentration in each open channel (i.e., with $\epsilon_{nm}^{(\mu)} \leq E_F$) at $T=0$ is simply given by[24]

$$n(E_F) = \frac{2n_\mu}{\pi}\sqrt{\frac{2m_x^{(\mu)}}{\hbar^2}\left(\frac{E_F(E_F+E_g)}{E_g}\right) - k_{nm}^{(\mu)2}}, \qquad (9)$$

where n_μ stands for the valley degeneracy. This shows that multivalley, anisotropy and nonparabolicity effects in PbTe NWs can be described by simple analytical solutions.

As for the L dependence, in Fig. 3 we compare the conductance obtained for NWs of different sizes. As expected, the onset of the conductance is shifted to lower Fermi energies as the wire width L increases due to the corresponding reduction in the size quantization. For a given increment in E_F, many more new states become occupied in wider wires, which explains the faster conductance increase seen in Fig. 3 for the wider NWs, and also the fact that wider conductance plateaus correspond to thinner NWs. Grabecki *et al.*[7] have measured the width dependence in the low-temperature conductance of PbTe NWs fabricated with submicron mesa constrictions on 12, 25, and 50 nm quantum wells. In the experiment, however, besides using [111] quantum wells, the conductance was measured as a function of the relative gate voltage, so that a direct comparison is not easy. Nevertheless, it is interesting to note that compared to their data (Fig. 2 in Ref. 7) the conductance shown in Fig. 3 as a function of E_F presents similar conductance step structure and wire width dependence.

The thermopower of single n-type [100] PbTe NWs at room temperature has been recently measured[25] as $S=-72$ μV/K. As a rough order of magnitude comparison, for a NW with the same electron concentration and cross-section area as that in Ref. 25, and neglecting high-temperature corrections,[17] we obtain $S=-170$ μV/K. For [110] NWs, approximate the same value is obtained, indicating a small NW crystallographic direction dependence.

Summarizing, the electronic conductance and Seebeck coefficients of 3D PbTe NWs have been calculated in the quantum transport regime, and studied as a function of the wire's dimension, temperature, and carrier concentration. The single-particle energy states were obtained analytically within the envelope-function approximation using Dimmock's four-band $k\cdot p$ model for the lead-salt bulk. The thermoelectric power of lead-salt NWs was shown to be characterized by irregular oscillations due to the intrinsic bulk band anisotropy and to the NW break of valley degeneracy. Lead-salt nanowires, in particular, PbTe NWs, are promising structures for new high-performance thermoelectric devices, and the present model with simple analytical expressions can help their development.

The authors acknowledge the support from the Brazilian agencies CAPES and CNPq, discussions with Professor R. Kishore and Professor G. C. La Rocca. E.A.A.S. would like to thank also the Scuola Normale Superiore di Pisa, Italy, where the present work was concluded, for the kind hospitality.

*erasmo@las.inpe.br

[1] L. D. Hicks and M. S. Dresselhaus, Phys. Rev. B **47**, 12727 (1993).
[2] L. D. Hicks and M. S. Dresselhaus, Phys. Rev. B **47**, 16631 (1993).
[3] J. P. Heremans, Acta Phys. Pol. A **108**, 609 (2005).
[4] S. Yuan, G. Springholz, G. Bauer, and M. Kriechbaum, Phys. Rev. B **49**, 5476 (1994).
[5] E. Abramof, E. A. de Andrada e Silva, S. O. Ferreira, P. Motisuke, P. H. O. Rappl, and A. Y. Ueta, Phys. Rev. B **63**, 085304 (2001).
[6] G. Grabecki, J. Wrobel, T. Dietl, E. Janik, M. Aleszkiewicz, E. Papis, E. Kaminska, A. Piotrowska, G. Springholz, and G. Bauer, Phys. Rev. B **72**, 125332 (2005).
[7] G. Grabecki, J. Wrobel, T. Dietl, E. Janik, M. Aleszkiewicz, E. Papis, E. Kaminka, A. Piotrowska, G. Springholz, and G. Bauer, Physica E **34**, 560 (2006).
[8] H. Beyer, J. Nurnus, H. Bottner, A. Lambrecht, T. Roch, and G. Bauer, Appl. Phys. Lett. **80**, 1216 (2002).
[9] T. Koga, T. C. Harman, S. B. Cronin, and M. S. Dresselhaus, Phys. Rev. B **60**, 14286 (1999).
[10] Y. M. Lin and M. S. Dresselhaus, Phys. Rev. B **68**, 075304 (2003).
[11] A. Popescu, L. M. Woods, J. Martin, and G. S. Nolas, Phys. Rev. B **79**, 205302 (2009).
[12] D. Rowe and C. Bandhari, *Modern Thermoelectrics* (Reston, Reston, VA, 1983).
[13] P. Streda, J. Phys.: Condens. Matter **1**, 1025 (1989).
[14] C. R. Proetto, Phys. Rev. B **44**, 9096 (1991).
[15] H. van Houten, L. W. Molenkamp, C. W. J. Beenakker, and C. T. Foxon, Semicond. Sci. Technol. **7**, B215 (1992).
[16] A. Lunde and K. Flensberg, J. Phys.: Condens. Matter **17**, 3879 (2005).
[17] R. Kim, S. Datta, and M. Lundstrom, J. Appl. Phys. **105**, 034506 (2009).
[18] J. O. Dimmock, in *The Physics of Semimetals and Narrow Gap Semiconductors*, edited by D. Carter and R. Bate (Pergamon, New York, 1971), p. 319.
[19] Note that this a mesoscopic approach. As the NW gets smaller, different effects neglected here start to be important, as local temperature variations and the thermopower dynamical formation. See, for instance, Y. Dubi and M. D. Ventra, Nano Lett. **9**, 97 (2009).
[20] Y. Nazarov and Y. M. Blanter, *Quantum Transport* (Cambridge University Press, New York, 2009).
[21] E. de Andrada e Silva, Phys. Rev. B **60**, 8859 (1999).
[22] T. N. Xu, H. Z. Wu, J. X. Si, and P. J. McCann, Phys. Rev. B **76**, 155328 (2007).
[23] R. Dalven, in *Solid States Physics: Advances in Research and Applications*, edited by F. Seitz, D. Turnbull, and H. Ehrenreich (Academic, New York, 1973), Vol. 28, p. 179.
[24] V. A. da Costa and E. de Andrada e Silva, in *Physics of Semiconductors*, edited by M. Caldas and N. Studart, AIP Conf. Proc. No. 1199 (AIP, Melville, NY, 2010) p. 289; notice that the values of the effective masses reported in this paper were unfortunately mixed-up.
[25] S. Jang, H. Kim, J. Park, M. Jung, J. Kim, S. Lee, J. Roh, and W. Lee, Nanotechnology **20**, 415204 (2009).